The 2009 IEEE/RSJ International Conference on
Intelligent Robots and Systems
October 11-15, 2009 St. Louis, USA

Motion Stabilization using Laser Distance Sensor for Biped Robots with Flexible Joint

Naoki Oda and Masanori Ito

Abstract— **This paper describes an approach of motion stabilization by using laser distance sensor for biped robots with flexible ankle joints. For avoiding the vibrated Zero Moment Point(ZMP) behavior due to the mechanical resonance, the vibration control method is proposed in the paper. The deviated center of gravity (COG) due to the ankle's deflection is measured in real-time by laser distance sensor, and equivalent reaction force relating to COG deviation is used as feedback signal for vibration control. The reaction force feedback also enables the regulation of the compliant property of the robots. Therefore the proposed approach is suitable to stabilize the walking behavior including the impact between foot and floor environments. The validity is evaluated by several experimental results.**

I. INTRODUCTION

Recently the biped robot technology have been developed remarkably, and studied from various viewpoints, such as mechanical design, stability, dynamics, passive walking, running motion and so on [1]-[6]. The dynamic stability can be evaluated by zero moment point (ZMP)[1], and currently ZMP is most appropriate and reliable index for biped motion stability [6]. In the past research, the linear inverted pendulum model (LIPM) has been proposed, and it's one of practical and powerful approach for generating stable walking pattern [7]. Generally, biped walking motion involves heavy interactions between robot and floor environments, and it is required that the rigid mechanical structure and flexible one exist together for impact-less stable walking.

However, the mechanical flexibilities make it difficult to track the desired ZMP trajectory. For example, sole or link deformation and joint torsion cause complicated ZMP movements. Therefore such deformations due to the the mechanical resonance is required to be small as much as possible under desired ZMP based trajectory. Otherwise it should be taken into account in the reaction force sensing strategy such as the detection of center of pressure(COP).

Generally, for obtaining the stable ZMP behavior, the motion in the acceleration dimension should be considered, because the ZMP depends on both the gravity and inertial force/moment. When the walking pattern is generated by LIPM, the sudden change of forward acceleration at the center of gravity (COG) is caused especially in the exchanging phase of supporting leg. Therefore, both the robust acceleration controlling and compliant property of contacting floor should be coped with in the motion controller.

N. Oda and M. Ito are with the Department of Opto-Electronic System Engineering, Chitose Institute of Science and Technology, Bibi, Chitose, Hokkaido, 066-8655, Japan, oda@photon.chitose.ac.jp, itou@odalab.spub.chitose.ac.jp

It is said that the impedance, or compliant control method is suitable for stabilizing the body[8], [9], [10]. However, in case of the robots with flexible joints, there is possibility that the vibrated behavior is occurred due to the natural mechanical resonance, and it is difficult to suppress such instability without vibration control. Then, from another view point, the reaction force received from ground environment is one of important indexes to stabilize the body. However the force or pressure sensor at the sole only works well when contacting flat on the ground.

From above mentioned view points, the authors have developed the walking motion controller by using laser distance sensor in past research[11], [12]. This paper focuses on the vibration control based on the laser-sensor without force sensor. In our approach, the deviated COG due to the ankle's deflection is directly measured in real-time by laser distance sensor, and the detected deflection is translated into the equivalent reaction force at COG. The feedback of reaction force in the same way of resonance ratio control[13], [14] is applied into the COG acceleration controller for vibration suppression. Since the deflection is directly used and fedback, the compliant property against the external force such as impact force from ground can be also regulated in the proposed controller. Furthermore its control performance does not so much depend on the foot condition of floor contact because of using optical sensing. Although the inertia sensor such as acceleration or gyro sensor, which can detect the absolute motion, may be available for same purpose, our approach based on laser distance sensor has an advantage that the precise deviation of COG due to the ankle joint flexibility is easily detectable under horizontal and even terrain floor.

The remainder of this paper is organized as follows. In Section II, the targeting robot model and the strategy based on laser sensor are presented. In Section III, the robust motion controller is designed by using disturbance observer technique, and the vibration suppression by resonance ratio controller is described in Section IV. The numerical simulations and experimental results are shown in Section V. Conclusions and future work are described in Section VI.

II. LASER-SENSOR BASED SENSING STRATEGY

The targeting biped robot has 12 DOF, each leg has 6 DOF as shown in Fig.1. For calculating COG, all links are assumed to be rigid, and mass model is given by Fig.1(b). The floor environment is assumed to be flat and horizontal. In this paper, the mechanical flexibilities exist in the ankle joints as shown in Fig.2(b). The supporting frame parts of ankle joint and foot parts connecting to the ankle don't have enough

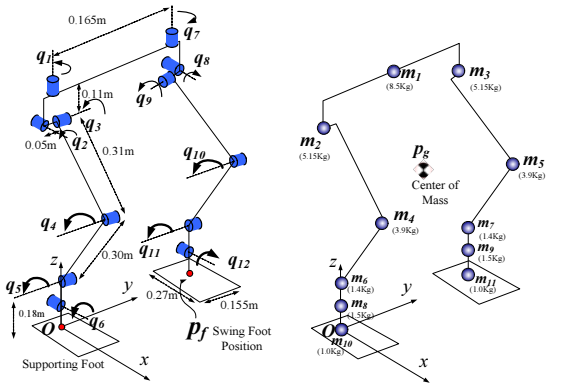

(a) 12 DOF Model (b) Mass Model

Fig. 1. Biped Robot Model

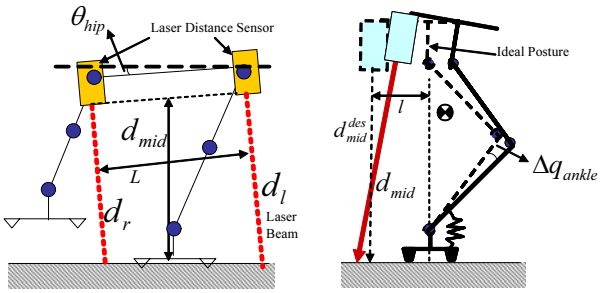

(a) Frontal View (b) Side View

Fig. 2. Laser Distance Sensor

stiffness. Therefore the deformation around ankle is naturally raised up in sagittal plane while walking. The deflection due to its flexibilities are detected by two laser distance sensor mounted on the hip plate as shown in Fig.2(a).

The actual angle of hip plate can be easily obtained from sensor outputs.

$$\theta_{hip} = \tan^{-1}\left(\frac{d_l - d_r}{L}\right) \tag{1}$$

where d_l and d_r are laser beam length of left and right sensor respectively, and L is the interval of two sensors. The vertical distance d_{mid} from sensor to floor around hip center can be obtained by using the mean value of sensor outputs.

$$d_{mid} = \frac{d_l + d_r}{2}\cos\theta_{hip} \tag{2}$$

The deflected angle Δq_{ankle} around ankle is calculated in the following equation.

$$\Delta q_{ankle} = \tan^{-1}\frac{d_{mid} - d_{mid}^{des}}{l} \tag{3}$$

Here d_{mid}^{des} means theoretical distance which is calculated from encoder signal with assuming all links and joints are rigid. And l is the gap length between ankle and sensor as shown in Fig.2(b), which can be also calculated from kinematic model.

The angle Δq_{ankle} can be approximately translated into the deviation of COG position with assuming the body is always near to upright.

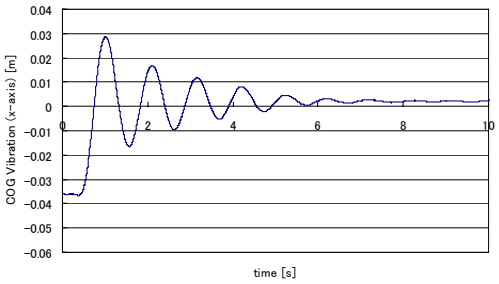

Fig. 3. An Example of the Vibrated Response Δx_g

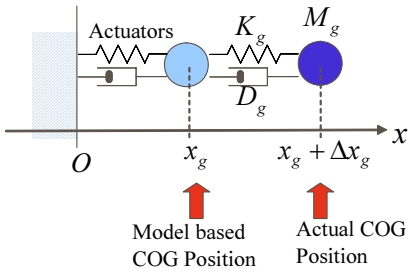

Fig. 4. Two Mass Spring Model of COG

$$\Delta x_g = z_g \tan\Delta q_{ankle} = \frac{z_g(d_{mid} - d_{mid}^{des})}{l} \tag{4}$$

Here COG position vector is defined as $\boldsymbol{p}_g = [x_g, y_g, z_g]^T$. The coordinate system in case support leg is right is shown in Fig.1. Actually, the foot is contacting to ground through four rubber bushes per foot attached on the sole, and then their minute vertical deformations are affected into getting the deviation Δx_g. Therefore, in our experiments, the deviation is calibrated with considering of the load distribution to the bushes. One more sensor will be meaningful for detecting the vertical deformation in future enhancements.

Figure 3 shows an example response of COG position under robust controlling stationary (the posture is as shown in Fig.2(a) and Fig.10(b), $z_g = 0.56$m). When pushing to backward direction and released after 0.5 sec, the measured deviation Δx_g by (4) is plotted in Fig.3. It is found that the ankle stiffness is not enough and it cause the shaking behavior due to the mechanical resonance. Therefor, the COG model in our approach is regarded as two mass spring system as shown in Fig.4. By using the natural response (Fig.3), the damping coefficients D_g and stiffness K_g were identified in case of actual Mass $M_g = 30$Kg as followings.

$$\begin{cases} M_g & = 30\text{Kg} \\ D_g & \approx 30\text{Ns/m} \\ K_g & \approx 1200\text{N/m} \end{cases} \tag{5}$$

III. Robust Motion Controller

In order to control both COG and swing foot motion independently, motion controller of a biped robot with 12

DOF includes two components: swing leg controller and COG ones.

The COG $\boldsymbol{p}_g$ and swing foot position $\boldsymbol{p}_f$ are defined as $[x_g, y_g, z_g]^T$ and $[x_f, y_f, z_f]^T$ respectively. The angles of hip and foot in Cartesian coordinates are controlled by using null space of Jacobian matrix. The position vectors $\boldsymbol{p}_f$ and $\boldsymbol{p}_g$ are obtained by calculating homogeneous transformation matrices.

$$\boldsymbol{p}_f = \boldsymbol{T}_f(\boldsymbol{q}) \tag{6}$$

$$\boldsymbol{p}_g = \boldsymbol{T}_g(\boldsymbol{q}) = \sum_{i=1}^{n} m_i \boldsymbol{p}_i / \sum_{i=1}^{n} m_i \tag{7}$$

Here the angle position vector $\boldsymbol{q} = [q_1, q_2, \cdots, q_{12}]^T$, and $\boldsymbol{p}_i$ is i-th mass position vector, n is total number of mass points. The velocity of foot position and COG can be represented as following formulations.

$$\dot{\boldsymbol{p}}_f = \boldsymbol{J}_f(\boldsymbol{q})\dot{\boldsymbol{q}} \tag{8}$$

$$\dot{\boldsymbol{p}}_g = \boldsymbol{J}_g(\boldsymbol{q})\dot{\boldsymbol{q}} \tag{9}$$

The matrix $\boldsymbol{J}_f \in \mathbb{R}^{3\times 12}$ and $\boldsymbol{J}_g \in \mathbb{R}^{3\times 12}$ mean the Jacobian matrix as follows:

$$\boldsymbol{J}_f(\boldsymbol{q}) = [\boldsymbol{j}_1 \;\; \boldsymbol{j}_2 \cdots \boldsymbol{j}_i \cdots \boldsymbol{j}_{12}] \tag{10}$$

where $\boldsymbol{j}_i = -\boldsymbol{e}_i \times (\boldsymbol{p}_f - \boldsymbol{r}_i)$.

$$\boldsymbol{J}_g(\boldsymbol{q}) = [\boldsymbol{j}_{g1} \;\; \boldsymbol{j}_{g2} \cdots \boldsymbol{j}_{gi} \cdots \boldsymbol{j}_{g12}] \tag{11}$$

where

$$\boldsymbol{j}_{gi} = -\boldsymbol{e}_i \times (\boldsymbol{x}_{gi} - \boldsymbol{r}_i) \cdot \sum m_k / \sum_{i=1}^{n} m_i \tag{12}$$

$$\boldsymbol{x}_{gi} = \sum m_k \boldsymbol{p}_k / \sum_{i=1}^{n} m_i \tag{13}$$

Here $\boldsymbol{r}_i$ is i-th joint position vector, and $\boldsymbol{e}_i$ is unit vector of rotational axis of i-th joint. And $\sum m_k$ and $\boldsymbol{x}_{gi}$ mean the sum of mass and COG in the flying foot side than i-th joint respectively.

The accelerations of swing foot and COG are obtained by time derivative of (8) and (9).

$$\ddot{\boldsymbol{p}}_f = \boldsymbol{J}_f(\boldsymbol{q})\ddot{\boldsymbol{q}} + \dot{\boldsymbol{J}}_f(\boldsymbol{q})\dot{\boldsymbol{q}} \tag{14}$$

$$\ddot{\boldsymbol{p}}_g = \boldsymbol{J}_g(\boldsymbol{q})\ddot{\boldsymbol{q}} + \dot{\boldsymbol{J}}_g(\boldsymbol{q})\dot{\boldsymbol{q}} \tag{15}$$

Finally the joint acceleration can be calculated from following equations.

$$\ddot{\boldsymbol{q}} = \boldsymbol{J}_f^{+}(\ddot{\boldsymbol{p}}_f - \dot{\boldsymbol{J}}_f\dot{\boldsymbol{q}}) + (\boldsymbol{I} - \boldsymbol{J}_f^{+}\boldsymbol{J}_f)\ddot{\boldsymbol{\phi}} \tag{16}$$

$$\ddot{\boldsymbol{q}} = \boldsymbol{J}_g^{+}(\ddot{\boldsymbol{p}}_g - \dot{\boldsymbol{J}}_g\dot{\boldsymbol{q}}) + (\boldsymbol{I} - \boldsymbol{J}_g^{+}\boldsymbol{J}_g)\ddot{\boldsymbol{\phi}}' \tag{17}$$

In angular acceleration control, the disturbance observer is applied for each joint in order to realize desired acceleration [14]. Additionally the workspace observer, which compensates the disturbance acceleration in workspace, is also integrated into foot and COG motion controller respectively to increase the robustness and decrease the computing costs of nonlinear coordinate transformations[15], [16]. The block diagram of workspace observer is shown in dashed box in Fig.5. Then the final calculations of angular accelerations are unified in (18).

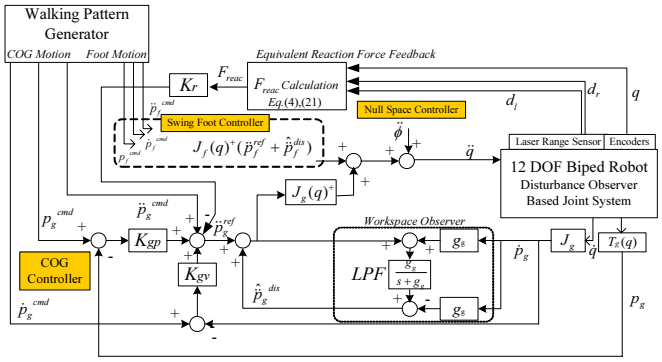

Fig. 5. Block Diagram of Proposed Controller

$$\ddot{\boldsymbol{q}} = \boldsymbol{J}_f^{+}(\ddot{\boldsymbol{p}}_f^{ref} + \hat{\ddot{\boldsymbol{p}}}_f^{dis}) + \boldsymbol{J}_g^{+}(\ddot{\boldsymbol{p}}_g^{ref} + \hat{\ddot{\boldsymbol{p}}}_g^{dis}) + \ddot{\boldsymbol{\phi}} \tag{18}$$

where $\ddot{\boldsymbol{p}}_f^{ref}$ and $\ddot{\boldsymbol{p}}_g^{ref}$ are reference inputs for foot and COG motion respectively, and $\hat{\ddot{\boldsymbol{p}}}_f^{dis}$ and $\hat{\ddot{\boldsymbol{p}}}_g^{dis}$ are estimated disturbances by workspace observers. In (18), $\boldsymbol{J}^{+}$ means the weighted pseudo inverse matrix $\boldsymbol{W}^{-1}\boldsymbol{J}^T(\boldsymbol{J}\boldsymbol{W}^{-1}\boldsymbol{J}^T)^{-1}$, in which $\boldsymbol{W}$ is weighting matrix. The last term of right hand side means null space factor, and $\ddot{\boldsymbol{\phi}}$ are arbitrary vector for using redundant degrees.

$$\ddot{\boldsymbol{\phi}} = \boldsymbol{K}_p^{null}(\boldsymbol{q}^{cmd} - \boldsymbol{q}) - \boldsymbol{K}_v^{null}\dot{\boldsymbol{q}} \tag{19}$$

where $\boldsymbol{K}_p^{null}$ and $\boldsymbol{K}_v^{null}$ are position and velocity feedback gains in null space motion. Equation (19) means posture constraints so that hip plate becomes parallel to both of supporting foot sole and swing foot one. When supporting leg is right, posture constraint command $\boldsymbol{q}^{cmd}$ is given by (20) in our approach.

$$\boldsymbol{q}^{cmd} = [0,\; -q_6,\; -q_4 - q_5,\; -,\; -,\; -,\; q_{yaw},\; -q_{12},\; -,\; -,\; q_{pitch},\; q_{roll}]^T \tag{20}$$

Here the angles q_{yaw}, q_{pitch}, q_{roll} are calculated value to be parallel with both supporting foot sole and swing foot one. And '$-$' means no constraint joint.

IV. Vibration Control for Stabilization

A. Equivalent Reaction Force Feedback

For stable sagittal motion response without mechanical resonance, the reaction force feedback, which is same approach of resonance ratio control proposed by [13][14], is integrated into COG controller.

In two mass model shown in Fig.4, the load side reaction force $\boldsymbol{F}_{reac}$ can be calculated from the deviation Δx_g obtained in (4).

$$\boldsymbol{F}_{reac} = [-K_g \Delta x_g,\; 0,\; 0]^T \tag{21}$$

The force $\boldsymbol{F}_{reac}$ is fed-back with scalar gain K_r in the motion controller.

$$\ddot{\boldsymbol{p}}_g^{ref} = \ddot{\boldsymbol{p}}_g^{cmd} + \boldsymbol{K}_{gp}(\boldsymbol{p}_g^{cmd} - \boldsymbol{p}_g) + \boldsymbol{K}_{gv}(\dot{\boldsymbol{p}}_g^{cmd} - \dot{\boldsymbol{p}}_g) - K_r\boldsymbol{F}_{reac} \tag{22}$$

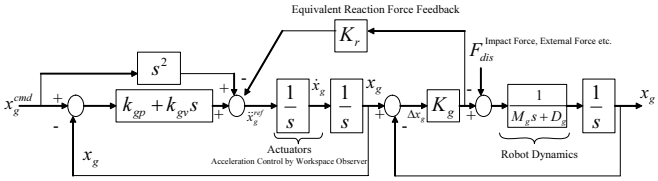

Fig. 6. Equivalent Block Diagram of Motion Controller

The acceleration reference of swing foot is simply given as next equation.

$$\ddot{\boldsymbol{p}}_f^{ref} = \ddot{\boldsymbol{p}}_f^{cmd} + \boldsymbol{K}_{fp}(\boldsymbol{p}_f^{cmd} - \boldsymbol{p}_f) + \boldsymbol{K}_{fv}(\dot{\boldsymbol{p}}_f^{cmd} - \dot{\boldsymbol{p}}_f) \tag{23}$$

Here $\boldsymbol{K}_{fp}$ and $\boldsymbol{K}_{gp}$ are position feedback gains, and $\boldsymbol{K}_{fv}$ and $\boldsymbol{K}_{gv}$ are velocity gains. The motion commands $\boldsymbol{p}_f^{cmd}$ and $\boldsymbol{p}_g^{cmd}$ are designed by using LIPM model as described subsection IV-C. The total block diagram is shown in Fig.5.

B. Control Parameter Design by Resonance Ratio Control

Assuming the ideal acceleration control by workspace observer, the equivalent block diagram from COG command to response in x-axis direction can be drawn by Fig.6. The transfer function from x_g^{cmd} to x_g can be obtained as followings in case of $D_g = 0$ for simplicity.

$$\frac{x_g}{x_g^{cmd}} = \frac{\omega_a^2(s^2 + k_{gv}s + k_{gp})}{s^4 + k_{gv}s^3 + (k_{gp} + \omega_m^2)s^2 + k_{gv}\omega_a^2 s + k_{gp}\omega_a^2} \tag{24}$$

where

$$\omega_a = \sqrt{K_g/M_g} \tag{25}$$

$$\omega_m = \sqrt{\frac{K_g}{M_g}(1 + K_r M_g)} = K\omega_a \tag{26}$$

$$K = \sqrt{1 + K_r M_g} \tag{27}$$

Here ω_a and ω_m are the natural frequency of the load side and motor side respectively. K is called resonance ratio in [13][14].

Next step, the denominator of (24) is determined for matching the motion performance described in (28).

$$D(s) = (s^2 + 2\zeta_1\omega_1 s + \omega_1^2)(s^2 + 2\zeta_2\omega_2 s + \omega_2^2) \tag{28}$$

In order to suppress the vibration, $\zeta_1 = \zeta_2 = 1.0$ for critical damping and $\omega_1 = \omega_2 = \omega_a$ for rapid response are selected here. Then, the control parameters k_{gp}, k_{gv} and K_r for COG controller in x-axis direction can be determined as followings by using the mechanical parameters (5).

$$\begin{cases} k_{gp} = & \omega_a^2 \approx 40 \\ k_{gv} = & 4\omega_a \approx 25 \\ K_r = & 4/M_g \approx 0.13 \end{cases} \tag{29}$$

C. Design of Walking Pattern by LIPM

The COG model for LIPM is illustrated as shown in Fig.7. Then the ZMP (x-axis direction) can be formulated as following equation.

$$x_{zmp} = x_g - \frac{z_g}{g}\ddot{x}_g \tag{30}$$

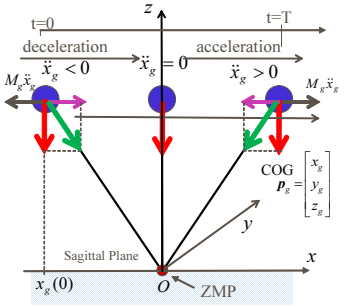

Fig. 7. Linear Inverted Pendulum Model (LIPM)

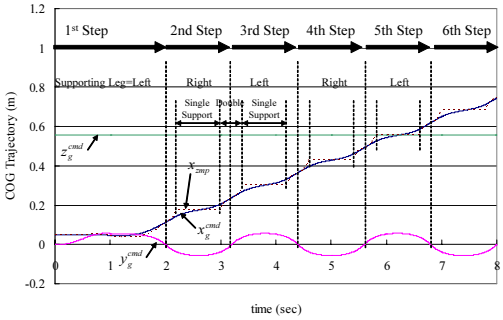

(a) COG Motion

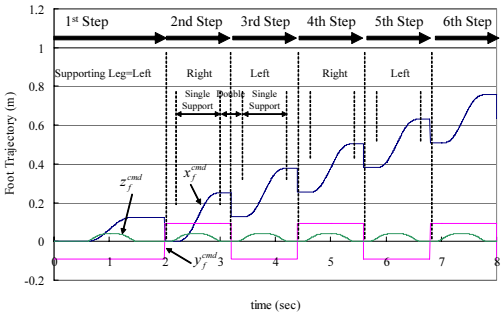

(b) Swing Foot Motion

Fig. 8. Designed Walking Pattern for Experiments

Here the constant g is gravity acceleration. The general solution for keeping the constant ZMP $x_{zmp} = 0$ can be obtained as next formulation.

$$x_g(t) = \frac{\dot{x}_g(0)}{\omega}\sinh\omega t + x_g(0)\cosh\omega t \tag{31}$$

where $x_g(0)$ and $\dot{x}_g(0)$ are desired initial position and velocity of COG, and $\omega = \sqrt{g/z_g}$. The COG trajectory in the swing phase is designed by using (31), and the trajectory in double support phase is generated by using the fifth order polynominal so as to satisfy the boundary condition between both phase. The foot and lateral motion are also designed by using fifth/eighth order polynominal and cosh functions respectively. The designed trajectory of COG and swing foot are plotted in Fig.8. The walking time cycle for one step is 1.2s (1st step is 2.0s) including the single support period 0.8s and double support period 0.4s. And step length is 0.25m (1st step is 0.125m), and peak height of flying foot for each step is 0.045m.

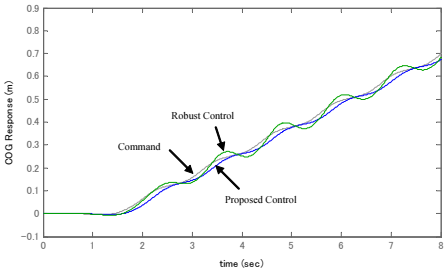

(a) COG Response

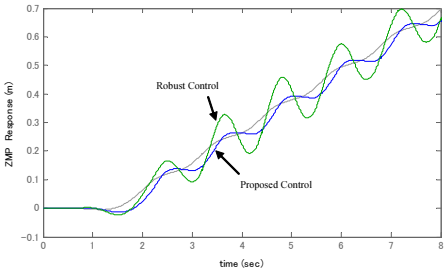

(b) ZMP Response

Fig. 9. Simulation Results of COG and ZMP Response

TABLE I

CONTROL PARAMETERS FOR EXPERIMENT

	Robust Control	Proposed Control
K_r	0.0	0.13
$\boldsymbol{K}_{fp}$	diag{2500,2500,2500}	
$\boldsymbol{K}_{fv}$	diag{100,100,100}	
$\boldsymbol{K}_{gp}$	diag{2500,2500,2500}	diag{40,2500,2500}
$\boldsymbol{K}_{gv}$	diag{100,100,100}	diag{25,100,100}
Observer Gain	g_g=100rad/s	
$\boldsymbol{K}_p^{null}$	diag{400,1600,2500,0,0,0, 400,400,0,0,1600,4900} in case support leg is right.	
$\boldsymbol{K}_v^{null}$	diag{40,80,100,0,0,0, 60,60,0,0,100,140} in case support leg is right.	
$\boldsymbol{W}$	diag{10,10,1,1,1,10,1,1,1,1,1,20} in case support leg is right.	

V. NUMERICAL AND EXPERIMENTAL RESULTS

A. Simulation

The performance of vibration suppression is evaluated by numerical simulation of the block diagram in Fig.6. When the trajectory x_g^{cmd} given by Fig.8(a) is used as input of Fig.6, the response x_g was calculated by MATLAB. The related control gains are listed in Table.I.

Fig.9 shows the COG and ZMP response. Although the some phase delay is appeared, the response is well tracked to the commanded waveform without oscillation. Then it is found that the ZMP behavior becomes the step-like response as shown in Fig.9(b).

B. Experimental Results

The validity of the proposed approach is confirmed by experimental results. Fig.10(a) shows a 12DOF biped robot for experiment. When standing upright, the hip height is 0.895m, and two laser distance sensors (Keyence LK-500) are mounted at hip plate (see Fig.10(b)) with $L = 0.41m$

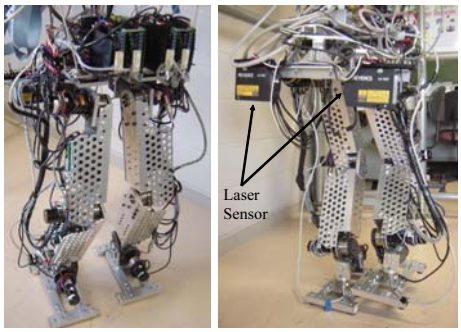

(a) Biped robot (b)Laser sensor

Fig. 10. 12 DOF Biped Robot

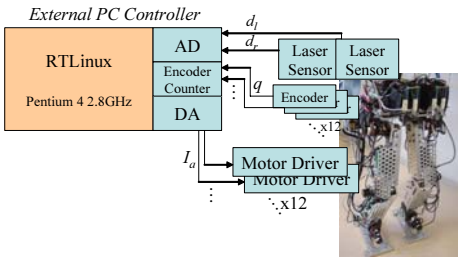

Fig. 11. Experimental Setup

interval and 0.69m height from floor to laser beam source. The detectable range by laser sensor is from 0.25m to 0.75m with 50μm resolution(Catalog Spec.). The total weight of the robot is approximately 35kg. Each joint is actuated by harmonic geared DC motor. The current commands for DC motors are supplied to motor drivers from external PC controller (OS: RTLinux). Experimental setup is shown in Fig.11. Control sampling time is 1ms.

Fig.12 shows the natural response against the external force. When pushing the robot manually and released in x-axis direction under controlling stationary (single leg supporting), the absolute COG position $x_g + \Delta x_g$ is plotted. In our approach, the remarkable effect of vibration suppression was successfully demonstrated. This results also mean that the stable and compliant property against the external disturbance can be achieved simultaneously.

Fig.13 shows the COG response while walking motion, which walking pattern is given by Fig.8. The plotted value is calculated from the sum of x_g and Δx_g. Under robust control, the resonant oscillation is gradually raised up. On the contrary, the COG response under proposed controller keep stable. In Fig.14, the estimated ZMP behavior is plotted. After two times differentiating the values plotted in Fig.13, the ZMP is estimated numerically by using (30). It is found that the vibrated behavior is smaller than robust control. However, since small discontinuous change is caused at switching coordinate system when exchanging the support leg, the estimated ZMP appeared large unreliable fluctuations. Therefore ZMP should be evaluated by force or pressure sensor in future work.

However, there are some weaknesses in our approach. Under uneven terrain surface, the detection of the joint

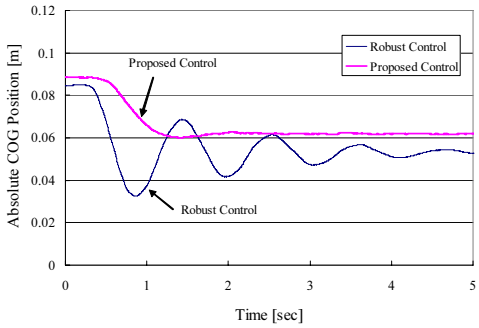

Fig. 12. Experimental Results of COG Vibration against External Force

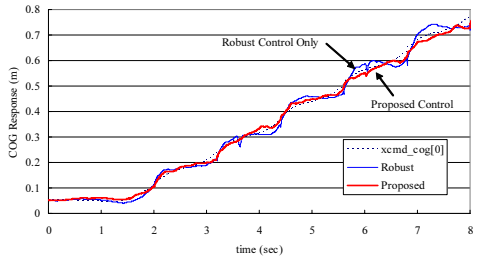

Fig. 13. Experimental Results of COG Response while Walking

ankle deformation may be difficult problem. The multi-sensor fusion should be considered for improving the adaptability under various floor environments. Furthermore, for fast walking motion, some additional enhancements will be required for stabilizing the ZMP behavior. Because the control performance depends on the resonant frequency due to the flexible joints, and it is difficult to track the desired COG trajectory under rapid walking. In such case, the momentum around COG may be also taken into account.

VI. Conclusions

The paper presented an approach of motion stabilization by using the laser distance sensor for biped robots with flexible ankle joints. The remarkable performance of vibration suppression was obtained in the simulation and experimental evaluations. The optical sensing approach may have the advantage in case of imperfect contact between the sole and floor. Furthermore, the feedback of the reaction force can be related to the compliance regulation against the external force. In our future work, the adaptive regulation of the feedback gain of the equivalent reaction force will be discussed for controlling both the vibration and compliance according to walking condition.

However, we have also several issues to be developed. For example, the control parameters designed by resonance ratio control does not contribute for making ZMP inside of stable foot print area. The additional posture regulator may be required. From the practical view point, the lateral motion and rough terrain issue should be considered in future study. Furthermore it is meaningful that the presented approach is combined with the actual sensing of the reaction force by force or pressure sensors.

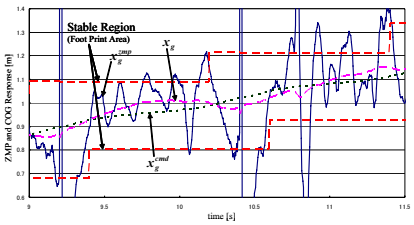

(a) Robust Control Only

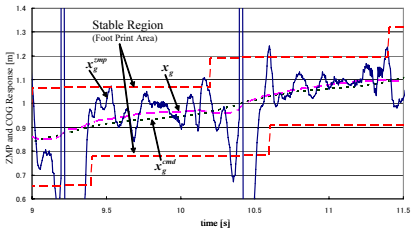

(b) Proposed Control

Fig. 14. Experimental Results of ZMP Response

References

[1] M. Vukobratovic, "How to Control Artificial Anthropomorphic Systems", *IEEE Trans. on Systems, Man and Cybernetics*, Vol.SMC-3, No.5, pp. 497–507, 1973

[2] T. McGeer, "Passive walking with knees", Proc. of IEEE Int. Conf. on Robotics and Automation, Vol.3, pp.1640–1645, 1990

[3] K. Hirai, M.Hirose, Y.Haikawa and T. Takenaka. "The development of honda humanoid robot". Proc. IEEE Int. Conf. Robotics and Automation, Vol.6, pp. 1321–1326, 1998

[4] Qiang Huang, et al. "Planning Walking Patterns for a Biped Robot". IEEE Trans. on Robotics and Automation, Vol.17, No.3, pp. 280–289, 2001

[5] Y. Fujimoto, "Trajectory Generation of Biped Running Robot with Minimum Energy Consumption". Proc. IEEE Int. Conf. Robotics and Automation, Vol.4, pp. 3803–3808, 2004

[6] S. Kajita, T. Nagasaki, K. Kaneko, H. Hirukawa, "ZMP-Based Biped Running Control", IEEE Robotics and Automation Magazine, Vol.14, No.3, pp.63–72, 2007

[7] S. Kajita, T. Yamaura, A. Kobayashi "Dynamic Walking Control of a Biped Robot Along a Potential Energy Conserving Orbit", IEEE Trans. on Robotics and Automation, Vol.8, No.4, pp.431–438, 1992

[8] J. H. Park, "Impedance Control for Biped Robot Locomotion". IEEE Trans. on Robotics and Automation, Vol.17, No.6, pp. 870–882, 2001

[9] T. Sugihara, Y. Nakamura, "Contact Phase Invariant Control for Humanoid Robot based on Variable Impedant Inverted Pendulum Model". Proc. of IEEE Conf. on Robotics and Automation, Vol.1, pp. 51–56, 2003

[10] S. Kawaji, K. Ogasawara, J. Iimori, S. Yamada, "Compliance Control of Biped Locomotion Robots", Proc. of IEEE Int. Conf. on Systems, Man, and Cybernetics, pp. 3801-3806, 1997

[11] N. Oda and H. Nakane, "An Approach of Motion Compensation for Biped Walking Robots with Structural Deformation", Int. Workshop on Advanced Motion Control, Vol.1, pp.278-283 , 2008

[12] N. Oda, T. Nagaki, M. Takigahira, "An approach of Hip Motion Compensation using Laser Range Sensor for Biped Walking Robot", Proc. IEEE Int. Conf. of Industrial Electronics Society (IECON2004), Vol.2, pp.1064–1069, 2004

[13] K. Yuki, T. Murakami, and K. Ohnishi, "Vibration Control of 2 Mass Resonant System by Resonance Ratio Control", Trans. IEE Japan, Vol. 113-D, No. 10, pp. 1162-1169 (1993-10) (in Japanese)

[14] K. Ohnishi, M. Shibata, T.Murakami, "Motion Control for Advanced Mechatronics", IEEE Trans. on Mechatronics, Vol.1, No.1, pp.56-67, 1996

[15] N. Oda, "Distributed Robust Motion Controller for Redundant Manipulator using Disturbance Observer", Journal of Robotics and Mechatronics, Vol.13, No.5, pp464-471, 2001

[16] T. Murakami, K. Kahlen, Rik. W.A.A. De Doncker, "Robust motion control based on projection plane in redundant manipulator". IEEE Trans. on Industrial Electronics, Vol.49, No.1, pp. 248–255, 2002